Research Article
Volume 11:03, 2022

Journal of Material Sciences & Engineering

ISSN: 2169-0022

Open Access

Temperature Dependent Properties of Electrodeposited $CuInTe_2$@ CdS Rod Like Heterostructures in Air and Argon Ambient

Manorama G. Lakhe* **and Nandu B. Chaure**

Department of Physics, Savitribai Phule Pune University, Pune, India

Abstract

$CuInTe_2$ (CIT) layers have been electrodeposited onto CdS coated FTO substrates at deposition potential -0.8 V verses Ag/AgCl reference electrode. The samples were annealed at four different temperatures *viz*, 350°C, 400°C, 450°C and 500°C for 20 minutes in air ambient, controlled argon ambient and Rapid Thermal Processesing (RTP) in presence of argon ambient for 5 shots. Samples were characterized by various characterization techniques to study structural, microstructural, morphological, compositional, chemical properties and concentration gradient of ionic species. Highly crystalline samples were obtained upon annealing the CIT layers in controlled argon ambient in tube furnace and RTP as a counter part of air annealed samples. Raman data shows removal of tensile strain upon annealing the samples in controlled argon ambient. Scanning Electron Microscopy (SEM) images shows increase in grain size for samples annealed at 350°C and 400°C in controlled argon atmosphere and in RTP. The high resolution Field Emission Scanning Electron Microscopy (FESEM) images shows further improvement in grain size in controlled argon atmosphere. Atomic Force Microscopy (AFM) images show rod like columnar morphology. XPS study shows the presence of Cu^+, In^{3+}, Te^{2-} and Te^{4+} states of copper, indium and tellurium. Time of Flight Secondary Ion Mass Spectroscopy (ToF SIMS) data shows almost uniform concentration of In and Te throughout the CIT layers annealed in controlled argon atmosphere. ToF SIMS data gives unique insight of concentration gradient of individual ionic species throughout the CIT layers and at CdS/CIT interface.

Keywords: Argon atmosphere • Rapid thermal processesing• Secondary phases• Time of flight

Introduction

The worldwide energy demand is constantly increasing and solar energy is one of the promising and clean sources of energy. Although silicon-based solar cells are the mainstay of today's photovoltaic industry; they are neither cheap nor optimal from materials perspective. Because of the primacy of silicon to the photovoltaic's industry researchers are in search of cost effective materials which will act as staple of the industry. Materials from chalcopyrite (I-III-VI_2) and family [1-3] may stand as an alternative to silicon because of their highest reported efficiency ~ 23.35% [4] for CIGS. $CuInTe_2$ (CIT) is also one of the successfully employed absorber material from chalcopyrite family mainly suitable for bottom cell applications in tandem solar cells because of its band gap in the IR region [5-9] and have reported highest efficiency 6.92% [9] by sophisticated MBE technique. To improve the efficiency, stability and ultimately the cell performance; evolution of microstructure during film/layer formation; reduction of secondary and volatile phases, removal of stresses and examining the distribution of ionic species throughout the layers has become the most important key factors in material/solar cell processesing [9-12]. Once material is obtained, normally processesing of the material starts with the annealing or heat treatment at higher temperature around 400°C to 600°C since it enables the formation of homogeneous and crack free material with significant crystalline grain growth [12-15]. In addition to that it is preferred to anneal the deposited layers in either argon or nitrogen [15-18] atmosphere at above mentioned temperature to get the desired phases. Next step after getting the desired phases examining the distribution of the ionic species throughout the layers in deposited film and film/substrate interface. In that sense ToF SIMS is an unique analytical technique to study the concentration gradient throughout the deposited layers and at sample-substrate interface, imaging and 3D tomography [19]. Number of researchers have used this technique very effectively to correlate the material/device properties as a function of chemical gradient of the deposited species [19-21]. In present study we report comparative results with clear change in crystallanity, microstructural properties, optical band gap, morphology, chemical composition, chemical states of ionic species and concentration gradient of individual ionic species throughout the CIT layers as a function of ambient conditions and annealing temperature on CdS coated FTO.

Materials and Methods

Experimental details

CIT layers have been electrodeposited at pH4 on CdS coated FTO substrate. The deposition parameters have already been optimized on CdS coated FTO substrate in our earlier work [22]. CIT layers deposited for 5 minutes were used for optical study, whereas thick layers deposited for 120 minutes were used for other characterization. Annealing of CIT layers is carried out from 350°C to 500°C for three different conditions such as, in air ambient in muffle furnace for 20 minutes, controlled argon ambient in tube furnace for 20 minutes and RTP in presence of argon ambient for 5 shots. The structural properties of CIT layers were studied by using X-ray diffractometer (model Bruker D8 Advance, Germany) with Cu Kα radiation with λ=0.154 nm. Invia Renishaw Raman Microscope coupled with Philips CCD camera was used to study the micro-structural properties. The semiconductor laser of wavelength 785 nm was used as an excitation source. Optical measurements were carried out by JASCO, UV-VIS-NIR Spectrophotometer model V-670. The surface morphology and elemental composition was studied by using SEM (JEOL JSM–6360 A SEM/EDAX) at an accelerating voltage 20 kV and probe current 1 nA. The plane surface morphology was also studied by using FESEM, Model HITACHI S4800 and 2D and 3D morphology by AFM Model-NSE (Nanoscope-E). In AFM study samples were scanned with contact mode using Si_3N_4 tip. The chemical states and composition was analyzed by X-ray photoelectron spectrophotometer using synchrotron source (Indus beam line–I ESCA-Electron spectroscopy for chemical analysis) spectrophotometer (Raja Ramanna Centre for Advanced Technology–(RRCAT), Indore, India). Al Kα radiation with energy 1486.6 eV was used for this study and hemispherical analyzer with 1 eV resolution and 50 eV pass-energy was used to detect the

---

***Address for Correspondence:** Manorama G. Lakhe, Department of Physics, Savitribai Phule Pune University, Pune, India; Tel: +9120 25692678; Email: lakhe.manorama@gmail.com*

Received: 26-Apr-2022, Manuscript No. JME-22-004-PreQc-22; **Editor assigned:** 29-Apr-2022, PreQC No. JME-22-004-PreQc-22 (PQ); **Reviewed:** 16-May-2022, QC No. JME-22-004-PreQc-22; **Revised:** 01-Jul-2022, Manuscript No. JME-22-004-PreQc-22 (R); **Published:** 01-Sep-2022, DOI: 10.37421/LMNC.2022.11.11

emitted photoelectrons. The elemental analysis is also carried out by using PHI TRIFT V nano Time of Flight Secondary Ion Mass Spectrometer. In ToF SIMS CIT samples were bombarded with high energy (30 kV) Ga^+ focused primary ion beams and analyzed with Cs sputter ion beam of energy (3 keV).

Results

X-ray diffraction

Figure 1 depicts the XRD pattern of as-deposited and air annealed CIT layers grown at -0.8 V versus Ag/AgCl reference electrode. A single piece of as-prepared sample was cut into several pieces and annealed at various temperatures ranging from 350°C to 500°C. Two broad peaks attributed around 2θ=22° to 26° and 38° to 50° in as-deposited samples are associated to the CIT reflection indicates the amorphous nature of CIT. The visible peaks marked by dark solid circles (•) corresponds to FTO substrate. An intense, well defined peaks of chalcopyrite CIT along with the secondary phases of Cu_xTe, CuO, In_2O_3, In_4Te_3 and elemental tellurium are exhibited in X-ray diffraction patterns of annealed CIT samples in an air ambient (Figures 1a-1d). Secondary phases are more prominent in the sample annealed at 450°C. Three prominent peaks of CIT corresponds to (112), (204)/(220) and (312)/(116) plane of tetragonal structure are observed in all annealed samples at 2θ=24.90o, 41.10° and 48.54° (JCPDS file no. 34-1498). The shift observed in XRD peaks ~ 0.25o in the annealed sample at 450°C is associated with tensile strain [23] developed upon heat treatment. The secondary peaks of Indium oxide (In_2O_3), (222), (400) and (440) planes (JCPDS file no. 74-1990) are observed in all air annealed samples along with indium telluride (In^4Te^3) reflections (311) and (351) (JCPDS file no. 29-0679). In addition, reflections related to $Cu_{1.75}Te$ (111), (311) and (200) (JCPDS file no. 45-1288), CuO (111), (200) (JCPDS file 80-1917) and elemental tellurium are also observed in air annealed samples. These peaks are marked in the XRD patterns. The presence of secondary phases of InTe and CuxTe are reported by Roy et al. [24] upon annealing CIT layers in graphite box. To remove secondary phases, as-deposited CIT layers grown at -0.8 V were annealed in tube furnace in continuous argon flow for temperatures ranging from 350°C to 500°C. The XRD pattern of CIT layers annealed in argon ambient from temperature 350°C, 400°C, 450°C and 500°C for 15 minutes is shown in Figures 2a-2e. It is revealed that the samples annealed in controlled argon ambient are highly crystalline and shows three prominent reflections of CIT at an angle 2θ=24.88°, 41.10° and 48.54° respectively. Secondary phases were not observed in the sample annealed at 400°C and 450°C whereas only one secondary phase of In_4Te_3 and In_2O_3 are present in the samples annealed at 350°C and 500°C, respectively. Broadening in the XRD pattern is observed in the samples annealed at 450°C and 500°C due to the unnuiform in particle size upon annealing (In SEM images small particle size has been observed and all the SEM micrographs are given in supporting information). Since very optimistic results were obtained for the samples annealed in controlled argon ambient, samples were further annealed in RTP furnace in argon ambient for 5 shots and results are shown in Figure 3. The crystallinity of the CIT samples annealed in RTP in presence of argon is nearly similar to that of the samples annealed in controlled argon ambient in tube furnace. All sample contains CIT reflections along with (311) plane of In_4Te_3 (Figures 3a-3e). In addition to this (222) plane of In_2O_3 is present in the sample annealed at 500°C. The broadening effect is also observed in the XRD pattern of the samples annealed at 350°C and 500°C. The sample annealed at 400°C for all the three conditions exhibits better results in terms of desired phases. Also, the secondary phases exhibited in air and RTP annealed samples are less prominent at 400ºC as compared to the samples annealed at other temperatures i.e. 350ºC, 450ºC and 500ºC. Therefore, 400ºC is found to be an optimum temperature. The summary of the standard and observed values of '2θ' and interplaner distance 'd' along with the FWHM for all the CIT samples is given in Table 1. In general broadening in the XRD peaks is due to the development of strain and uneven crystallite size.

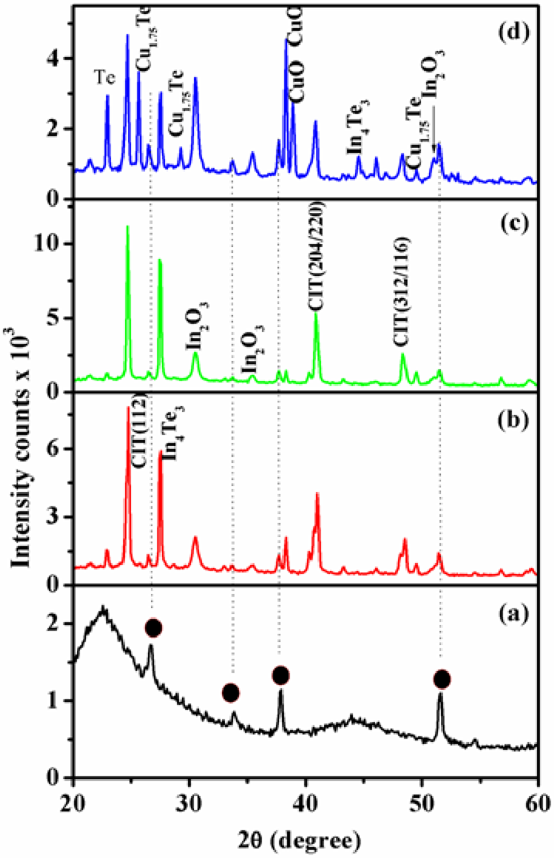

Figure 1. XRD patterns for (a) as-deposited sample deposited at -0.8 V and corresponding annealed CIT samples at (b) 350°C, (c) 400°C and (d) 450°C in air ambient in muffle furnace.

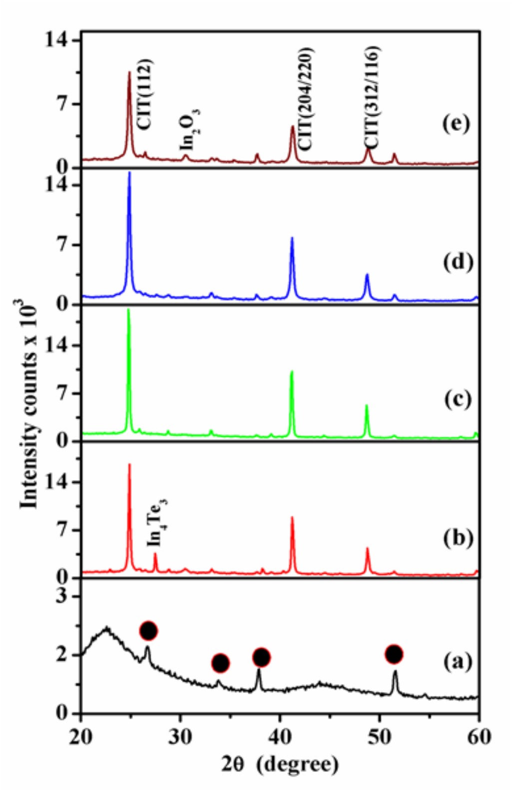

Figure 2. XRD patterns for (a) as- deposited sample deposited at -0.8 V and corresponding annealed CIT samples at (b) 350°C, (c) 400°C, (d) 450°C and (e) 500°C in controlled argon ambient in tube furnace.

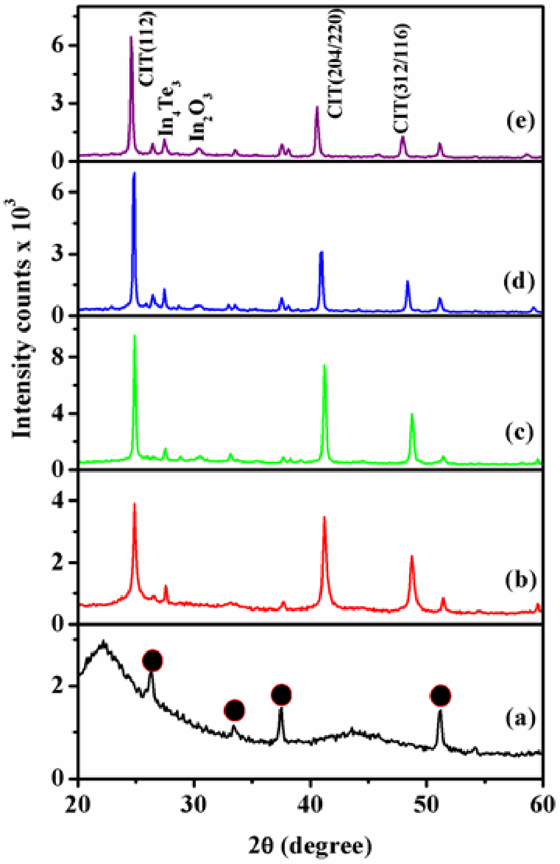

Figure 3. XRD patterns for (a) as- deposited sample deposited at -0.8 V and corresponding annealed CIT samples at (b) 350°C, (c) 400°C, (d) 450°C and (e) 500°C in argon ambient in RTP in argon ambient.

Table 1. Summary of standard and observed values of angle '2θ', interplaner distance 'd' and FWHM for the samples annealed from 350°C to 500°C in air ambient, controlled argon ambient and RTP in argon ambient for 5 shots.

Annealing temperature			**Air ambient**			**Controlled argon ambient**			**RTP in presence of argon ambient**		
(°C)	'2θ' (A°)	'd'	'2θ' (A°)	'd' FWHM		'2θ' (A°)	'd' FWHM		'2θ' (A°)	'd' FWHM	
	Standard		Observed			Observed			Observed		
350	24.86	3.581	24.77	3.598	0.14	24.87	3.581	0.09	24.87	3.581	0.13
	41.18	2.192	40.98	2.200	0.13	41.11	2.193	0.11	41.18	2.190	0.17
	48.71	1.869	48.53	1.875	0.17	48.73	1.866	0.13	48.73	1.866	0.19
400	24.86	3.581	24.67	3.606	0.13	24.87	3.581	0.12	24.87	3.581	0.10
	41.18	2.192	40.88	2.206	0.18	41.18	2.190	0.15	40.97	2.203	0.12
	48.71	1.869	48.34	1.882	0.19	48.73	1.866	0.18	48.33	1.882	0.12
500	24.86	3.581	-------	-------	-------	24.87	3.591	0.15	24.56	3.623	0.11
	41.18	2.192	-------	-------	-------	41.27	2.187	0.21	40.58	2.222	0.14
	48.71	1.869	-------	-------	-------	48.83	1.864	0.26	47.94	1.896	0.17

The combined effect of both strain and crystallite size on the Full Width at Half Maximum (FWHM) is calculated by the Williamson–Hull (W–H) equation [25,26]

$$\beta \cos\theta = \eta \sin\theta + \lambda / t$$

where 'β' is the average value of FWHM diffraction peaks, 'θ' is the Bragg diffraction angle, 'η' is the strain, 'λ' is the wavelength of CuKα line (1.54 A°) and 't' is the average crystallite size.

Figure 4 shows the plot of βcosθ verses sinθ for all the CIT samples annealed in (A) air ambient, (B) controlled argon ambient and (C) RTP in presence of argon ambient. The strain is calculated from the slope and inverse of the intercept gives the crystallite size. The values of crystallite size calculated for CIT (112) peak by Debye Scherer formula and Williamson–Hull equation along with strain are summarized in Table 2. The crystallite size is found to be larger at 350°C and 400°C for the samples annealed in controlled argon ambient and RTP in presence of argon. It is observed that the crystalline size systematically decreases with increasing annealing temperature (except the crystalline size calculated for the air annealed sample by Debye Scherer formula) which is also consistent with SEM images given in supporting information. The strain calculated for CIT samples annealed for three different conditions with different temperatures are found to be positive, indicates the presence of effective tensile strain [23]. There is no systematic change in the strain however more strain is calculated for air annealed samples at 350°C and 400°C, in controlled argon annealed samples at 450°C and 500°C and in RTP at 350°C and 500°C because of the lattice mismatch at sample-substrate interface during recrystallization of CIT grains [25]. As samples annealed at 400^{o}C shows optimum results, further characterization is carried out at this temperature for all the three annealing conditions (Figure 4).

Table 2. Crystallite size and strain calculated for the samples annealed in air ambient, controlled argon ambient and RTP in presence of argon from 350°C to 500°C.

Temperature (°C)	**Crystallite size (nm) calculated by Debye Scherer formula**			**Williamson- Hull analysis Crystallite Size (nm)**			**Strain x 10^{-3}**		
	Air	**Argon**	**RTP**	**Air**	**Argon**	**RTP**	**Air**	**Argon**	**RTP**
350	59	91	63	66	93	91	6.42	4.1	4.02
400	74	81	82	85	92	91	6.14	2.85	2.46
450	63	68	82	73	77	84	3.97	4.83	2.12
500	--	53	71	--	62	57	-----	7.09	4.16

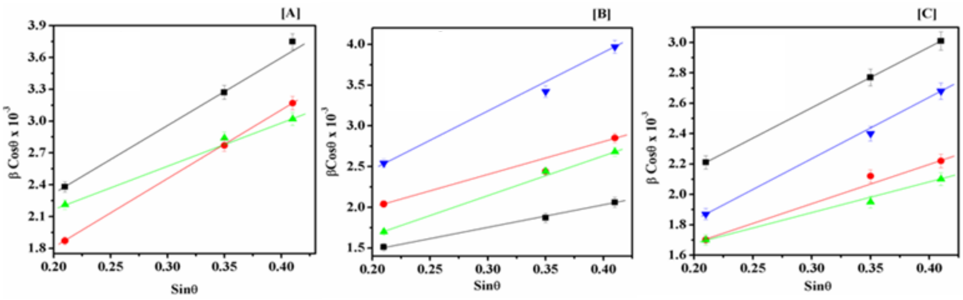

Figure 4. Plot of βcosθ verses sinθ for CIT samples annealed in (A) air ambient, (B) controlled argon ambient and (C) in RTP in presence of argon ambient, **Note:**(■) 350°C; (●) 400°C; (●) 450°C; (●) 500°C.

Discussion

Raman spectroscopy

Figures 5a-5d depicts the Raman shift for 5 % laser power for (a) as-deposited and annealed CIT samples at 400°C, (b) air ambient in muffle furnace, (c) controlled argon ambient in tube furnace and (d) RTP in argon ambient respectively. All the details of Raman modes of CIT is explained in our previous results [8,22]. From Figure 5, the most prominent modes; A1 (standard frequency 123 cm^{-1}), B1 (standard frequency 143 cm^{-1}) and E and B2 (267 cm^{-1}) are present in all CIT samples with shift in their original peak positions. The RED shift is observed in the entire CIT spectrum which indicates the development of tensile strain [27,28], except the sample annealed in argon ambient. FWHM is also found to be decreased for sample annealed in argon ambient as compared to as-deposited and samples annealed in air and RTP. The broad hump ranging from 150 cm^{-1} to 185 cm^{-1} is due to the mixing of E4 (LO or TO) at 158 cm^{-1}, E5 or B2 (TO and LO) at 171 cm^{-1} and 182 cm^{-1} respectively. The peak at 185 cm^{-1} is more prominent in air annealed samples. The broad humps with very weak intensity at 215 cm^{-1} to 220 cm^{-1} is the combination of E and B2 modes, which is present in all samples. We have also varied laser power from 0.2% to 10.0% and Raman modes as a function of laser power and shift in frequencies as compared to their standard frequencies for all laser power are summarized in Table 1, S_1 in supporting information and explained Elsevier [8,22]. From Figure 4 S_1 it is clearly observed that Raman intensity increases with increase in laser power. Photon flux directly affects the charge transfer which changes the band structure and electronic insertion and shows the effect on Raman intensity [29]. Also some of the modes become distinguishable for specific laser power whereas some of the mode becomes silent. This clearly shows that number of photons/photon flux changes the possibility of Raman transitions. It is also noticed that depending upon laser intensity there is small shift in the peak positions due to the change in bond strength, interatomic distance and atomic substitution [29]. Increase in Raman peak intensity and decrease in broadening with increase in temperature is also reported by Su, et al. [30]. In present data, the change in annealing ambient shows change in Raman intensity and shift in peak positions especially in air annealed sample due to the incorporation of defect and secondary phases which eventually affects on phonon lifetime (Figure 5) [31,32]. The improvement in crystal quality and strain is further modified upon argon annealing in tube furnace and rapid thermal annealing in RTP furnace which is also reflected in S_1.

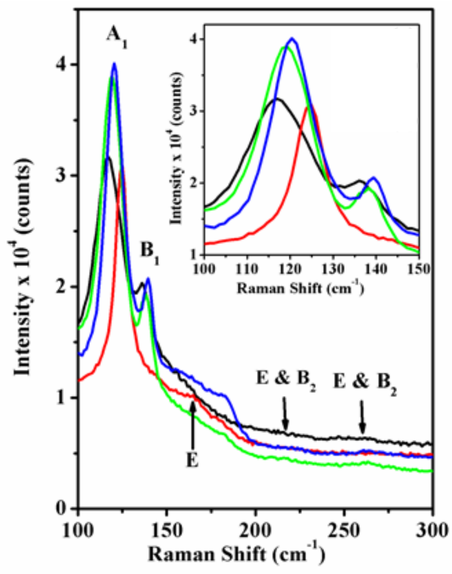

Figure 5. Raman spectra for (a) as-deposited sample deposited at -0.8 V and corresponding annealed CIT samples at 400°C in (b) air ambient, (c) argon ambient and (d) in RTP in presence of argon ambient. **Note:** (—) (a); (—) (b); (—) (c); (—) (d).

Even for a constant laser power it is observed that the peak position of Raman modes shifted towards low wave number for as-deposited, air and RTP annealed sample and this red shift is proposed due to the development of tensile strain. In case of argon annealed sample Raman modes are observed at their original position and FWHM is found to be minimum which clearly indicates that removal of tensile strain and good crystalline quality of the CIT sample.

UV-Visible-IR spectroscopy

Optical measurements were performed on (a) as-deposited and annealed CIT layers at 400°C in (b) air ambient, (c) controlled argon ambient and (d) RTP in argon ambient and shown in Figures 6a-6d.

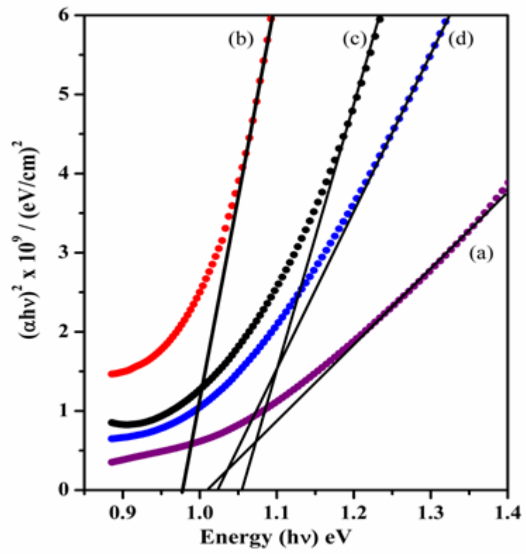

Figure 6. Plot of (α hν)2 verses energy (hν) of (a) as-deposited sample deposited at -0.8 V and corresponding annealed CIT samples at 400°C in (b) air ambient, (c) argon ambient and (d) in RTP in argon ambient.

For this study CIT layers were deposited for 5 minutes. The band gap of as-deposited film was found to be 1.02 eV. The band gap estimated after annealing of CIT layers varies from 0.97 eV (air ambient) to 1.05 eV (argon ambient) with change in absorption intensity. The change in band gap is because of the change in crystallinity and chemical composition upon annealing. Obtained band gap values of CIT samples are nearly similar to the reported literature values [5-9,33].

Scanning Electron Microscopy (SEM)

The surface morphology of CIT samples annealed from 350°C to 500°C for 15 minutes for three different conditions; i) air ambient, ii) controlled argon ambient and iii) RTP in presence of argon ambient studied by SEM is given in supporting information in S_2, S_3 and S_4 respectively and explained in details. It is also observed that after annealing, CIT layers become more compact in presence of argon ambient. From XRD results, the optimum results are obtained at 400°C for all three conditions therefore as-deposited sample and samples annealed at 400°C for three different conditions are further examined by Field Emission Scanning Electron Microscopy (FESEM) and Atomic Force Microscopy (AFM).

Field Emission Scanning Electron Microscopy (FESEM)

FESEM images of as-deposited and annealed CIT samples at 400°C in air ambient in muffle furnace, controlled argon ambient in tube furnace and in RTP in argon ambient is shown in Figures 7a-7d. Compact CIT layers were deposited with fully covering the substrate. Upon annealing sample grain size decreases in air ambient as well as in RTP whereas increases in argon ambient in tube furnace with grain size ~ 1 µm. Globular cauliflower like morphology is observed for all conditions with change in grain size.

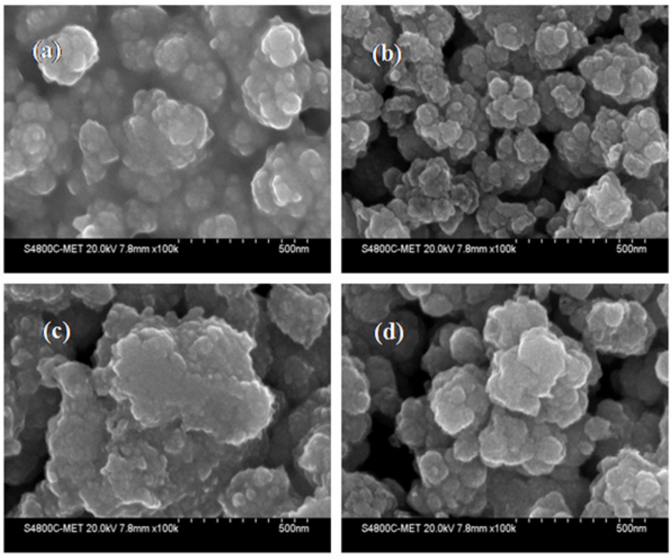

Figure 7. FESEM Images of (a) as-deposited sample deposited at -0.8 V and annealed CIT samples at 400°C in (b) air ambient, (c) controlled argon ambient and (d) in RTP in argon ambient.

Atomic Force Microscopy (AFM)

Two dimensional AFM images for 1 µm x 1 µm magnification of (a) as-deposited and annealed CIT samples at 400°C for three different conditions; (b) air ambient, (c) controlled argon ambient and (d) RTP in presence of argon is shown in Figures 8a-8d. Inset shows images taken at 5 µm x 5 µm. Columnar growth of CIT has been observed in as-deposited sample on CdS coated FTO substrate with layer by layer agglomeration of the CIT grains to form the rods. After annealing the samples, growth remains columnar but rods converted into thick planer sheets as shown in Figure 8. The width of rods is found to be ~ 300 nm in as-deposited sample whereas after annealing it increased to ~ 500 nm.

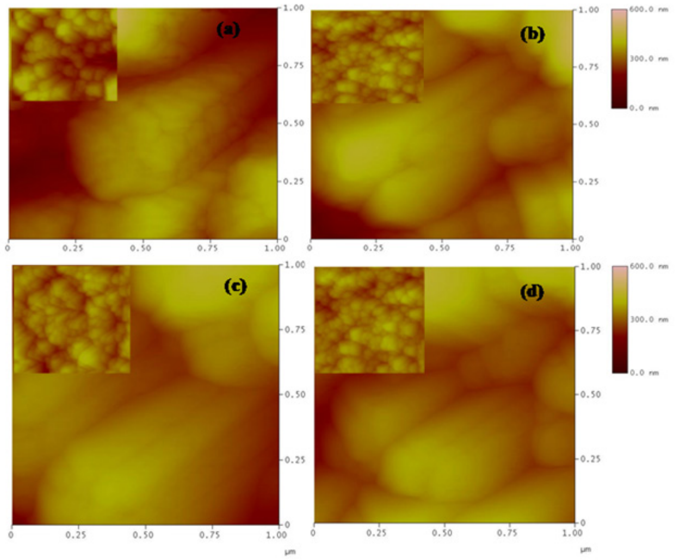

Figure 8. Two dimensional AFM images of (a) as-deposited sample deposited at -0.8 V and corresponding annealed CIT samples at 400°C in (b) air ambient, (c) controlled argon ambient and (d) in RTP in argon ambient.

Figure 9 shows three dimensional AFM images of the same samples given in Figure 8. Columnar rods like morphology is confirmed in the as-deposited sample. Upon annealing, its orientation changes for all conditions. The morphology of the CIT rods has found to be tampered in case of controlled argon ambient, and RTP. The surface roughness increases upon annealing and air annealed sample was found to be more rough as compared to others.

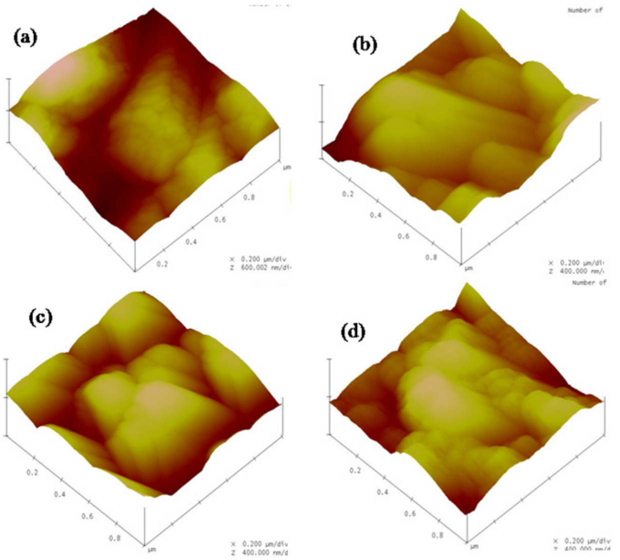

Figure 9. Three dimensional AFM images of (a) as-deposited sample deposited at -0.8 V and corresponding annealed CIT samples at 400°C in (b) air ambient, (c) controlled argon ambient and (d) in RTP in argon ambient.

Energy dispersive spectroscopy

Elemental analysis of the CIT samples were carried out by EDS assembly attached with SEM and summarized in Table 3. From EDS data it is observed that all annealed layers are indium-rich. Copper concentration has found to be increased systematically in air annealed samples whereas decreased in RTP. No systematic change has been observed in copper concentration for samples annealed in controlled argon ambient. Also no particular trend noticed in indium concentration with increase in temperature in air and controlled argon annealed samples however it decreased systematically with increase in temperature upon RTP annealing. Tellurium concentration remains similar for controlled argon annealed samples and systematically increased with increase in temperature for RTP. Cu/In ratio is sufficiently small enough i.e. less than 0.5 which is expected for the development of high efficiency solar cells [7,9] and also decreased systematically with increase in annealing temperature for RTP and air. CIT layer/film does not sustain at 500°C in air ambient.

X-ray photoelectron spectroscopy

The chemical states and composition of as-deposited and annealed CIT sample in controlled argon ambient in tube furnace at 400°C was analyzed by X-Ray photoelectron spectrophotometer. Prior to the experiment, the samples were sputter-cleaned with an Ar$^+$ ion beam (2 kV, 10 nA) till the surface oxide peaks were no longer observed in the XPS spectra. Gold 4 f$_{7/2}$ line with the binding energy 83.8 eV was used for calibration.

Figure 10 shows the core level spectrum of (a) as-deposited CIT and (b) the same sample annealed in argon ambient. Individual XPS spectrum of Cu, In and Te species and its peak positions is depicted in Figure 11a for as-deposited CIT sample and Figure 11b for corresponding argon annealed sample in tube furnace. The present data is compared with the standard literature data [34-36].

In detailed survey scan carbon (1S) and oxygen (1S) line is present at 285 eV [34-36] and 530 eV [34-38] respectively in both CIT samples. From individual XPS data Cu 2p$_{3/2}$ and Cu 2p$_{1/2}$ lines arises at 932.2 eV and 952.1 eV in as-deposited CIT sample and at 932.6 eV and 952.2 eV in corresponding argon annealed sample (Figure 11) [34-38]. From Figure 10, In 4d$_{3/2}$ line is observed at 17.7 eV [34]. In 3d$_{5/2}$ line arises at 444.4 eV in as-deposited CIT and 444.1 eV [34-37] in argon annealed CIT. In 3d$_{3/2}$ line arises at 451.9 eV in as-deposited CIT and 451.6 eV [34-37] in argon annealed CIT respectively. In addition from Figure 10, In 3p$_{3/2}$ line arises at

665.6 eV [34], In $3p_{1/2}$ line arises at and 703.4 eV in as-deposited CIT and at 704.0 eV [34] in argon annealed CIT, respectively. From Figure 10, Te $4d_{5/2}$ and Te $4d_{3/2}$ lines are observed at 40.2 eV and 43.5 eV [34,39] in both CIT samples. From Figure 10 it is observed that TeO_2 (Te IV) peaks are present in both CIT samples and arises at 576 eV [34, 35] and 586.4 eV [34,40] respectively. Te $3d_{5/2}$ line arises at 572 eV whereas Te $3d^{3/2}$ line arises at 582.6 eV [34-37,39] in both CIT samples. The Te(IV) state was found to be more prominent, indicates easy oxidation property of tellurium. Te $3p_{3/2}$ and Te $3p_{1/2}$ lines are also observed in both CIT samples at 822.5 eV and 873.7 eV [34] respectively.

As CIT layers were deposited on CdS coated FTO, cadmium lines i.e. Cd $3d_{3/2}$ and Cd $3d_{5/2}$ are also present and observed at 411.1 eV and 404.7 eV [34,40] in argon annealed sample. Thus XPS data shows presence of Cu^+, In^{3+}, Te^{2-} and Te^{4+} states of copper, indium and tellurium in CIT samples and Cd^{2+} contributed from the substrate (CdS coated FTO).

Table 3. Summary of elemental composition of (a) as-deposited sample deposited at -0.8 V and corresponding air annealed samples in muffle furnace, argon annealed samples in tube furnace and RTP in presence of argon at (b) 350°C, (c) 400°C, (d) 450°C and (e) 500°C in argon ambient in tube furnace and RTP in argon ambient.

Temperature (°C)	Elemental composition in atomic wt%											
	Air				Argon				Argon (RTP)			
	Cu	In	Te	Cu/In	Cu	In	Te	Cu/In	Cu	In	Te	Cu/In
350	10	35	55	0.28	13	33	54	0.39	17	33	50	0.51
400	11	39	50	0.28	12	34	54	0.35	15	34	51	0.44
450	12	33	55	0.36	14	32	54	0.43	13	32	55	0.40
500	-------	-------	-------	------	11	34	55	0.32	12	31	57	0.38

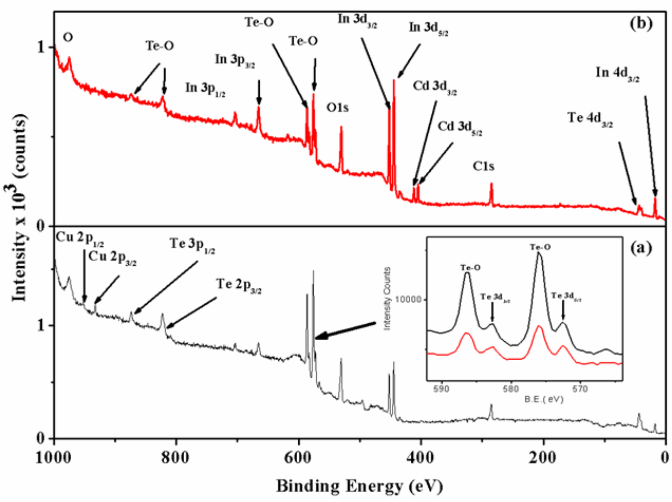

Figure 10. The core level spectrum of (a) as-deposited sample deposited at -0.8 V and corresponding (b) annealed CIT in argon ambient in tube furnace.

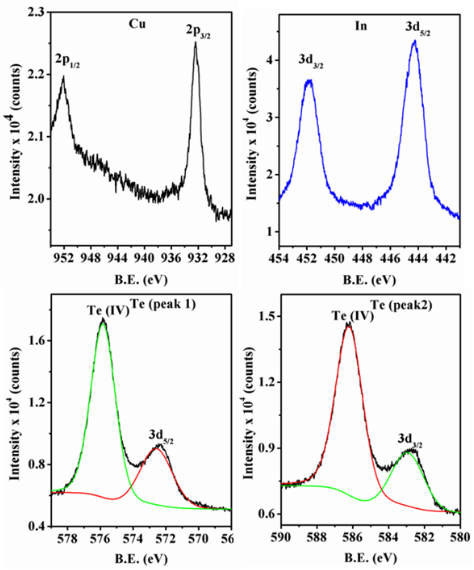

Figure 11a. Individual XPS spectrum of the Cu, In and Te species and its peak positions for as-deposited CIT sample deposited at -0.8 V.

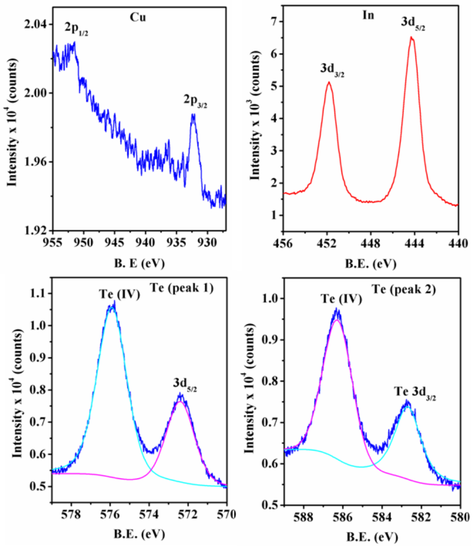

Figure 11b. Individual XPS spectrum of the Cu, In and Te species and its peak positions for annealed CIT sample in argon ambient in tube furnace at 400°C, deposited at -0.8 V.

Time of Flight Secondary Ion Mass Spectroscopy (ToF SIMS)

The qualitative elemental analysis of as-deposited and annealed CIT layers for three different conditions; i) air ambient in muffle furnace, ii) controlled argon ambient in tube furnace and iii) RTP in presence of argon is carried out by Time of Flight Secondary Ion Mass Spectrometer and shown in Figure 12. CIT samples were bombarded with 30 keV primary Ga^+ ion gun and various atomic species are ejected into vacuum chamber in which a very small amount (~ 1%) of charged species of Cu, In, Te and Na are emitted as a secondary ions and extracted in the flight tube by operating in either positive/negative polarity mode. Ionic species with positive oxidation states will be extracted by applying negative potential. In present case Cu^+, In^{3+}, Te^{2+}, Na^+ is extracted into flight tube. Depth profiling is carried out by high flux low energy Cs ion (~ 3 keV) beam with above charged species and shown in Figures 12a-12d. All the basics of ToF SIMS in details has been explained in detail by Harvey, et al., [20]. In present case there is un-uniform distribution of all ionic species throughout the CIT layers in as-deposited sample. Whereas CIT layers annealed in air and argon ambient, initially the indium count decreases for ~ 1 second and then suddenly increases and remains uniform throughout the layers and again decreases at the material substrate interface. Tellurium count is less and shows almost similar pattern for all the samples. Very small copper count is observed in ToF SIMS spectrum may be because of re-oxidation of copper. The similar is true with tellurium species. The signal for tellurium is expected to be double as that of indium but it is less because during the sputtering there are formation of positive and negative oxidation states of the tellurium and only positive states were detected by the SIMS detector. The states carrying negative charge were not detected by ToF SIMS detector since an instrument is operated in negative polarity mode while extraction. In all samples comparable sodium count is observed in SIMS spectrum may be because of two possible reasons i) Na might have incorporated in CIT layers since prior to deposition of CIT, pH of the bath solution was adjusted with NaOH pellets and ii) during higher temperature annealing some trace amount of Na from substrate might have diffused in CIT layers. It is well reported in literature that addition of alkaline earth metals [41,42], especially Na and K plays a positive role for the development of high efficiency solar cell. Since Soda Lime Glass Substrate (SLG) contains reasonable amount of Na, it diffuses into the CIGS layer during the growth of CIGS and improves the electronic properties of the final device. Chirila, et al. [41] showed the effect of potassium induced surface modification of CIGS surface and developed 20.4% efficient solar cell on flexible polymide substrate. They have also given the SIMS profile for the CIGS solar cells treated with Na and K and showed that optimum amount of Na and K incorporation enhances the solar cell properties. In present study it is clearly observed that sodium count is quite high in the order of ~ 105 and need to optimize to improve electronic properties for device application. The CCD image of the CIT sample during the sputtering is also shown in Figure 12. This particular depth profile study will help us in optimization of material properties during deposition and K/Na treatment to enhance the electronic properties and ultimately the optimum cell performance. Further investigation is needed to optimize the deposition parameters as well as annealing conditions to get uniform concentration gradient throughout the absorber layers.

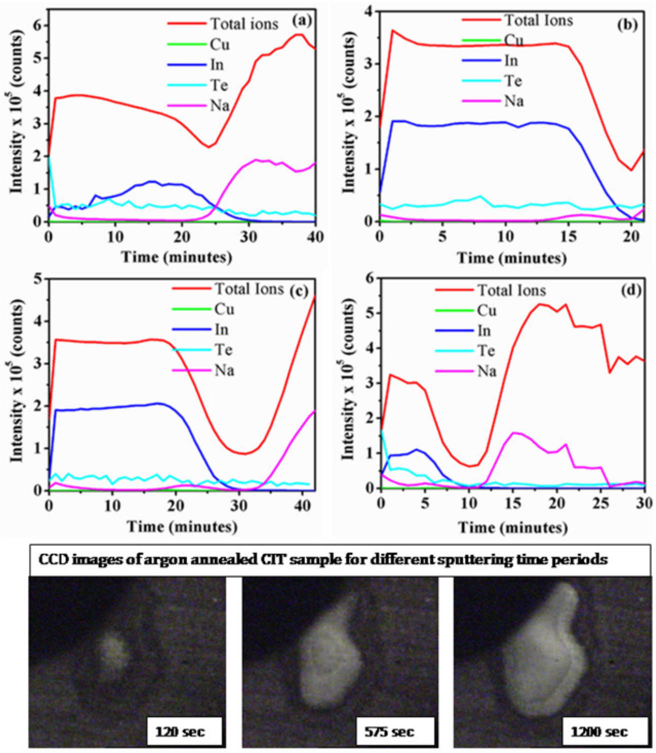

Figure 12. ToF SIMS spectra of CIT samples deposited on CdS coated FTO substrate; (a) as-deposited at -0.8 V, (b) annealed in air ambient, (c) controlled argon ambient and (d) in RTP in argon ambient. **Note:** (—) Total Ions; (—) Cu; (—) In; (—) Te; (—) Na.

Conclusion

In this study optimization of CIT layers is carried out on CdS coated

FTO and results are summarized as follows.

Highly crystalline samples were obtained on CdS coated FTO and degree of crystallanity of argon and RTP annealed CIT layers has found to be increased by ~ 3 to 4 times more than the heat treated samples reported in our previous articles. No secondary phases were observed in samples annealed in controlled argon ambient at 400°C and 450°C.

Raman data shows removal of tensile strain upon argon annealing. The band gap of the CIT samples varies from 0.90 eV to 1.09 eV and well agreed with the literature. SEM and FESEM images confirmed globular morphology and showed increase in grain size in argon annealed CIT layers in tube as compared to air and RTP and found to be ~ 1 µm under FESEM for the samples annealed at 400°C. AFM study confirms the columnar growth and rod like morphology of CIT layers with increased grain size upon annealing. Indium rich CIT layers were deposited and Cu/In ratio found to varies in between 0.28 to 0.50 which is reported to be optimum from solar cell perspective. XPS study shows presence of Cu^{+}, In^{3+}, Te^{2-} and Te^{4+} states of copper, indium and tellurium in CIT samples. ToF SIMS results shows almost nearly similar distribution of ionic species in air and controlled argon annealed CIT layers as compared to as-deposited and RTP annealed CIT. Thus higher temperature CIT annealing especially carried out in controlled argon ambient gives optimum results in terms of crystalline quality, morphology, Cu/In ratio and uniform concentration of indium throughout the layers but further investigation and optimization is needed during deposition to incorporate optimum amount of sodium incorporation and improve the interfacial properties in terms of solar cell device.

Acknowledgements

One of the authors ML is thankful to University Grant Commission (UGC) for Basic Scientific Research (BSR) fellowship. We gratefully acknowledge Prof. B.B. kale from CMET Pune for allowing us to use FESEM facility and Prof. D. C. Kothari from Mumbai University for Raman Spectroscopy.

References

1. Liu, W, Li H, Qiao B and Zhao, et al. “Highly Efficient CIGS Solar Cells Based on A New CIGS Bandgap Gradient Design Characterized by Numerical Simulation.” *Solar Energy* 223 (2022): 337-334.
2. Jseng, Y, Chaob C, Sungc H and Chen T. “CIGS Thin Film and Device Performance Produced through a Variation Ga Concentration During Three-Stage Growth Process.” *Mater Sci Semicond Process* 87 (2018): 162-166.
3. Jackson, P, Hariskos D, Wuerz R and Kiowski O, et al. “Properties of Cu (In, Ga) Se2 Solar Cells with New Record Efficiencies up to 21.7%.” *Phys Status Solidi* 9 (2015): 28-31.
4. Green, MA, Dunlop ED, Hohl-Ebinger J and Yoshita M, et al. “Solar Cell Efficiency Tables (Version 56).” *Prog Photovolt Res Appl* 28 (2020): 629-638.
5. Ishizaki, T, Saito N, and Fuwa A. “Electrodeposition of CuInTe2 Film From an Acidic Solution.” *Surface and Coatings Technology* 182 (2004): 156-160.
6. Muftah, G, Samantilleke A, Warren P and Heavens S. “Electrochemical Deposition of CuInTe2 Layers For Applications in Thin Film Solar Cells.” *Journal of Materials Science: Materials in Electronics* 21(2010): 373-379.
7. Mise, T and Nakada T, “Microstructural and Optical Properties of CuIn3Te5 Thin Films For Solar Cells” *Solar Energy Materials and Solar Cells* 94 (2010) :1132-1136.
8. Lakhe, M and Chaure NB, “Characterization of Electrochemically Deposited CuInTe2 Thin Films for Solar Cell Applications.” *Solar Energy Materials & Solar Cells* 123 (2014): 122-129.
9. Mise, T and Nakada T, “Narrow-Bandgap CuIn3Te5 Thin-Film Solar Cells.” *Prog Photovolt: Res Appl* 21 (2013): 754-759.
10. Hibberd, CJ, Ganchev M, Kaelin M and Dann SE. “Structural Properties of Cu(In,Ga)Se2 Thin Films Prepared From Chemically Processed Precursor Layers.” *Thin Solid Films* 517 (2009): 2235-2239.
11. Park, SJ, Lee E, Jeon HS and Ahn SJ. “A Comparative Study of Solution Based CIGS Thin Film Growth on Different Glass Substrates.” *Applied Surface Science* 258 (2011): 120-125.
12. Todorov, T and Mitzi DB. “Direct Liquid Coating of Chalcopyrite Light-Absorbing Layers for Photovoltaic Devices.” *Eur J Inorg Chem* 2010 (2010): 17-28.
13. Zhang, L, Zhuang D, Zhao M and Gong Q. “The Effects of Annealing Temperature on CIGS Solar Cells by Sputtering From Quaternary Target with Se-Free Post Annealing.” *Applied Surface Science* 413 (2017): 175-180.
14. Song, Z, Watthage SC, Phillips AB and Tompkins BL, et al. “Impact of processing temperature and composition on the formation of Methylammonium lead iodide perovskites” *Chem Mater* 27 (2015): 4612 – 4619.
15. Flammini, MG, Debernardi N, Ster ML and Dunne B, et al. “The influence of heating time and temperature on the properties of CIGSSe solar cells” *Int J Photener*, 2016 (2016): 1-7.
16. Souici, FZ, Benhaoua B, Saidi H and Boujmil MF, et al. “Influence of rapid thermal annealing in argon atmosphere on properties of electrodeposited CuInSe2 thin films: Structural and optical study” *Chalco Letters* 16 (2019): 79-87.
17. Fernandes, PA, Salome PMP, da Cunha AF, and Schubert B. “Cu2ZnSnS4 solar cells prepared with sulphurized dc-sputtered stacked metallic precursors” *Thin Solid Films* 519 (2010): 7382.
18. Sousa, MG and da Cunha AF, “High SnS phase purity films produced by rapid thermal processing of RF-magnetron sputtered SnS2-x precursors” *Appl Sur Sci* 472 (2019): 64-70.
19. Matteocci, F, Busby Y, Pireaux J and Divitini G, et al. “Interface and Composition Analysis on Perovskite Solar Cells” *ACS Appl Mater Interfaces* 7 (2015): 26176–26183.
20. Harvey, SP, Messinger J, Zhu K and Luther JM, et al. “Investigating the Effects of Chemical Gradients on Performance and Reliability within Perovskite Solar Cells with TOF-SIMS.” *Adv Energy Mater* (2020): 1903674.
21. Harvey, S, Li Z, Christians JA and Zhu K, et al “Probing perovskite inhomogeneity beyond the surface: Tof-Sims analysis of halide perovskite photovoltaic devices” *ACS Appl Mater Interfaces* 10 (2018): 28541–28552.
22. Lakhe, M, Mahapatra SK, and Chaure MB. “Development of CuInTe2 thin film solar cells by electrochemical route with low temperature (80oC) heat treatment procedure” *Materials Science and Engineering B* 204 (2016): 20–26.
23. Rohom, AB, Londhe PU and Chaure NB. “The effect of pH and selenization on the properties of CuInSe2 thin films prepared by electrodeposition technique for device applications” *J Solid State Electrochem*, 19 (2015): 201-210.
24. Roy, S, Guha P, Chaudhuri S and Pal AK, “CuInTe2 thin films synthesized by graphite box annealing of In/Cu/Te stacked elemental layers” *Vacuum* 65 (2002): 27.
25. Chaure, S, Chaure NB and Pandey RK. “Electric Field Assisted Growth of Self-Organized CdS Films: Size Dependent Structural and Optical Properties” *J Nanosci Nanotechnol* 7 (2007): 945.
26. Chaure, S, Chaure NB and Pandey RK. “Self-assembled nanocrystalline CdSe thin films” *Physica E: Low-dimensional Systems and Nanostructures* 28 (2005): 439-446.
27. Wolf ID. “Micro-Raman spectroscopy to study local mechanical stress in silicon integrated circuits” *Semicond Sci Technol* 11 (1996): 139.
28. Sahoo, S, Sharma GL and Katiyar RS. “Raman spectroscopy to probe residual stress in ZnO nanowire” *J Raman Spectrosc* 43 (2012): 72.
29. Gouadec, G and Colomban P. “Raman Spectroscopy of Nanomaterials: How Spectra Relate to Disorder” Particle Size and Mechanical Properties” *Prog Crystal Growth and Characterization of Materials* 53 (2007): 1.
30. Su, Y, Zhang T, Zhang P and Jiang J, et al. “Effects of Annealing Temperature on Raman Scattering and Electrical Properties of Te-Doped Nanostructured Black Silicon.” *J Materials Sci Res* 2 (2013): 34-41.
31. Choudhury, B and Choudhury A. “Local Structure Modification and Phase Transformation of TiO2 Nanoparticles Initiated by Oxygen Defects, Grain Size, and Annealing Temperature.” *Int Nano Lett* 3 (2013): 55.
32. Wu, K, and Wang D. “Temperature-Dependent Raman Investigation of CuInS2 with Mixed Phases of Chalcopyrite and CuAu.” *Phys Status Solidi A* 208 (2011): 2730-2736.
33. Lakhe, MG, and Chaure NB. “Transport Properties of CuInTe2 Thin Films Obtained by the Electrochemical Route.” *J Electron Mater* 47 (2018): 7099-7105.

34. Wagner, CD, Riggs WM, Devis LE and Moulder JF, et al. “Handbook of X-Ray Photoelectron Spectroscopy, Perkin-Elmer Corporation, Physical Electronics Division USA.” (1979).
35. Kim, S, Kang M, Kim S and Heo JH et al. “Fabrication of CuInTe2 and CuInTe2-xSex Ternary Gradient Quantum Dots and Their Application to Solar Cells.” *ACS Nano* 7 (2013): 4756.
36. Kuriakose, L, Simi NJ and Ison VV. “CuZn2InTe4 Quantum Dots-A Novel Nanostructureemploying A Green Synthesis Route.” *RSC Adv* 10 (2020): 18560-18564.
37. Kim, C, Kim DH, Son YS and Kim H, et al. “Solvothermal Synthesis and Characterization of a CuInTe2 Absorber for Thin-Film Photovoltaics.” *Materials Res Bull* 47 (2012): 4054.
38. Akgul, FA, Akgul G, Yildirim N and Unalan HE, et al. “Influence of Thermal Annealing on Microstructural, Morphological, Optical Properties and Surface Electronic Structure of Copper Oxide Thin Films. *Materials Chem Phys* 147 (2014): 987.
39. Grisaru, H, Palchik O and Gedanken A. “Microwave-Assisted Polyol Synthesis of CuInTe2 and CuInSe2 Nanoparticles.” *Inorg Chem* 42 (2003): 7148-7155.
40. Osial, M, Widera J and Jackowska K. “Influence of Electrodeposition Conditions on the Properties of CdTe Films”. *J Solid State Electrochem* 17 (2013): 2477-2486.
41. Chirila, A, Reinhard P, Pianezzi F and Bloesch P, et al. “Potassium-Induced Surface Modification of Cu(In,Ga)Se2 Thin Films for High-Efficiency Solar Cells.” *Nat Materials* 12 (2013): 1107-1111.
42. Jackson, P, Wuerz R, Hariskos D, and Lotter E, et al. “Effects of Heavy Alkali Elements in cu(in,Ga)Se2 Solar Cells with Efficiencies up to 22.6%.” *Phys Status Solidi RRL* 10 (2016): 583-586.

How to cite this article: G. Lakhe, Manorama and Nandu B. Chaure. “Temperature Dependent Properties of Electrodeposited CuInTe2@CdS Rod Like Heterostructures in Air and Argon Ambient.” *J Material Sci Eng* 11 (2022): 11.